Electronic Supplementary Material (ESI) for ChemComm.

Supporting Information

Polyoxometalate-Organic Supermolecular Nanotube with High Chemical Stability and Proton-Conducting Properties

Gao-Juan Cao,[a,b] Jing-Dong Liu,[a] Ting-Ting Zhuang,[a] Xiu-Hong Cai,[a] and Shou-Tian Zheng*[a]

[a]College of Chemistry, Fuzhou University, Fuzhou, Fujian 350108, China.

[b]Department of Applied Chemistry, College of Life Science, Fujian Agriculture and Forestry University, Fuzhou, Fujian 350002, China

This file includes:

Section S1 Synthesis and Methods

Synthesis of 1: $Na_9[A\text{-}\alpha\text{-}PW_9O_{34}]\cdot nH_2O$ (PW_9) were prepared by literature method (*Inorganic Syntheses*, John Wiley & Sons: New York, 1990, vol.*27*, *p*85). A mixture of PW_9 (0.300 g), $Ni(NO_3)_2\cdot 6H_2O$ (0.350 g) and 1H-1,2,4-triazole-3-thiol (0.050 g) was added into 4 mL of a 0.5 M sodium acetate buffer (pH 4.8). Further, 0.20 mL en was added to this solution and stirred for half an hour, transferred into a Teflon-lined stainless steel autoclave (25 mL) and kept at 170 °C for 3 days, and then cooled to room-temperature. After washed by water and ethanol, green crystals were obtained. Anal. Calcd (Found %) for $C_{16}H_{71}N_{19}Ni_5O_{44}PS_3W_9$: C, 6.08 (5.81); H, 2.46 (2.16); N, 7.86 (8.03).

Single-crystal structure analysis: Crystals were collected on a Bruker APEX II diffractometer at room temperature equipped with a fine focus, 2.0 kW sealed tube X-ray source (MoK radiation, λ = 0.71073 Å) operating at 50 kV and 30 mA. The empirical absorption correction was based on equivalent reflections. Structures were solved by direct methods followed by successive difference Fourier methods. Computations were performed using SHELXTL and final full-matrix refinements were against F^2. All non-hydrogen atoms were refined anisotropically. Due to highly porous structure of **1**, the guests (including about four diprotonated H_2en molecules and six water molecules per formula evaluated by the results of CHN analysis and TGA) within structure are highly disordered and thus couldn't be exactly determined. The contribution of these disordered solvent molecules to the overall intensity data of all structures were treated using the SQUEEZE method in PLATON. CCDC-1030121 contains the supplementary crystallographic data for this paper. These data can be obtained free of charge from The Cambridge Crystallographic Data Centre via www.ccdc.cam.ac.uk/data_request/cif.

Gas adsorption measurements: We tried to active the as-synthesized **1** by different strategies. One way is that, considering compound **1** is stable up over 200 °C and TGA shows the loss of neutral guests is completed at about 150 °C, the as-synthesized **1** (about 130 mg, denoted as sample **1**) was directly degassed at 180 °C for 48 h under vacuum prior to the measurement. Another way is that, considering compound **1** is also stable in low-boiling solvent of methanol, a copy of new sample (about 130 mg, denoted as sample **E1**) was refluxed in a saturated methanol solution of NH_4Cl for 48 h to exchange relatively high-boiling guests of organic amines and water with attempt to move away guests at relatively lower temperature. However, the TGA of

the guest-exchanged sample **E1** shows the loss of neutral guests is still completed at about 150 ^{o}C (Figure S3), which indicates the incorporated organic amines and water are hard to be exchanged completely. Nevertheless, in order to make a comparison with sample **1,** sample **E1** was still degassed at relatively lower temperature (80 ^{o}C) for 48 h under vacuum prior to the gas adsorption measurement. Additionally, we also tried to detect the porosity of both samples by utilizing different kinds of gases including H_2, CO_2, and N_2. All gas adsorption measurements were performed on a Micromeritics ASAP 2020 surface-area and pore-size analyzer from 1.0 Torr to atmospheric pressure. N_2 and H_2 adsorptions were measured at 77 K, while CO_2 adsorption was measured at 273k. Though different activation methods were tried, both samples exhibit similar but poor gas adsorption properties for all testing gases (Figure S8-S10). The N_2 sorption measurements indicate both samples have a low uptake over the entire pressure range (16.4 cm^3/g for sample **1** and 14.2 cm^3/g for sample **E1** at 1atm). The BET surface areas evaluated by N_2 adsorptions are 30.6 m^2/g and 29.7 m^2/g for samples **1** and **E1**, respectively. It is noteworthy that the BET surface areas are low, especially much lower than those porous metal-organic frameworks (MOFs), but they are analogous to many reported porous structures based on polyoxometalates as building blocks (e.g. compounds in *CrystEngComm*, 2010, **12**, 1880, 1765, *Inorg. Chem*, 2013, **52**, 2662, *Inorg. Chem*, 2014, **53**, 7309, and *Angew. Chem. Int. Ed*, 2014, **53**, 3608). Both samples also have a low uptake of CO_2 at 1 atm (8.6 cm^3/g for sample **1** and 5.3 cm^3/g for sample **E1**), which almost can be negligible. Further H_2 sorption measurements indicate samples **1** and **E1** can also adsorb a small amount of H_2 at 1 atm (20.5 cm^3/g for sample **1** and 18.0 cm^3/g for sample **E1**).

Others: Powder XRD patterns were obtained using a RIGAKU-Miniflex II diffractometer with Cu *Kα* radiation (λ = 1.54056 Å).. Elemental analyses (C, H and N) were performed by using a Vario EL III elemental analyzer. IR spectra were recorded on PerkinElmer Spectrum One FT-IR infrared spectrophotometer with pressed KBr pellets in the range of 4000-400 cm^{-1}. Thermal analyses were performed in a dynamic air atmosphere with a heating rate of 10 ºC/min, using a NETZSCH STA 449C thermal analyzer. Variable temperature susceptibility measurements were carried out in the temperature range 2-300 K at a magnetic field of 0.1T on polycrystalline samples with a Quantum Design PPMS-9T magnetometer. The experimental susceptibilities were corrected for the Pascal's constants. Ac impedance measurements were carried out with a zennium/IM6 impedance analyzer over the frequency range from 0.1 Hz to 5 MHz with an applied voltage of 50mV. The relative humidity was controlled by a STIK Corp. CIHI-150B

incubator. The samples were pressed to form a cylindrical pellet of crystalline powder sample (~3 mm thickness ×5 mm ϕ) coated with C-pressed electrodes. Two silver electrodes were attached to both sides of pellet to form four end terminals (quasi-four-probe method). The bulk conductivity was estimated by semicircle fittings of Nyquist plots.

BVS calculations (I. D. Brown, D. Altermatt, *Acta Crystallogr., Sect.* **1985**, *B41*, 244) for **1** reveal that the oxidation states of all W and Ni are +6 and +2, respectively. For oxygen atoms, the bond valences of the three μ_3-O atoms (-1.089 – -1.094) from the Ni_4O_4 core and the terminal oxygen atom (0.242) on the capping Ni^{2+} ion suggest they are OH and H_2O, respectively. Except the above oxygen atoms, the oxidation states of all the other oxygen atoms (-1.760 – -2.150) are identified as -2 by BVS calculations. Thus the overall charge of **1a** polyoxoanion is -8. In order to balance the charge of **1a**, four isolated en molecules included into structure through EA and TG analysis were considered as diprotonated guests, which are exactly consistent with the overall charge balance of **1**.

Section S2 Additional tables

Table S1. Hydrogen bonds for **1** [Å and º].

D-H...A	d(D-H)	d(H...A)	d(D...A)	<(DHA)
N(1)-H(1B)...O(20A)	0.90	2.28	3.126(11)	156.4
O(1W)-H(1WA)...O(19A)	0.85	2.02	2.714(11)	138.0
O(1W)-H(1WB)...O(19B)	0.85	2.02	2.714(11)	138.0

Symmetry transformations used to generate equivalent atoms: A: y, -x+y, -z+1; B: y, -x+y, z-1/2

Section S3 Additional Structural Figures

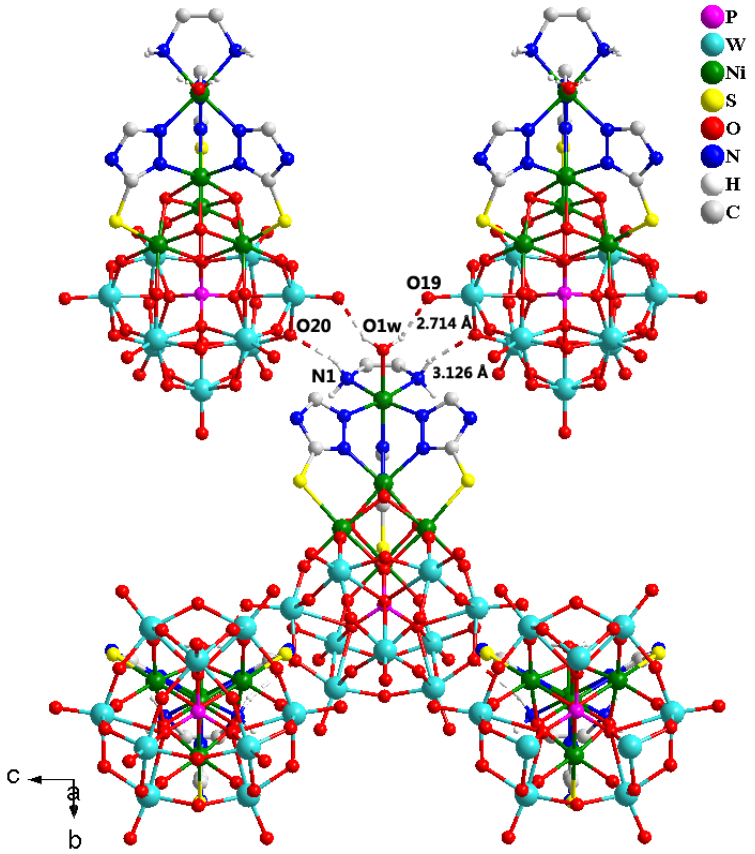

Figure S1. View of hydrogen bonds among the Ni_5-subsitiuted polyoxotungstates, showing each Ni_5-subsitiuted polyoxotungstate connected to four neighboring ones via OH···O and NH···O interactions.

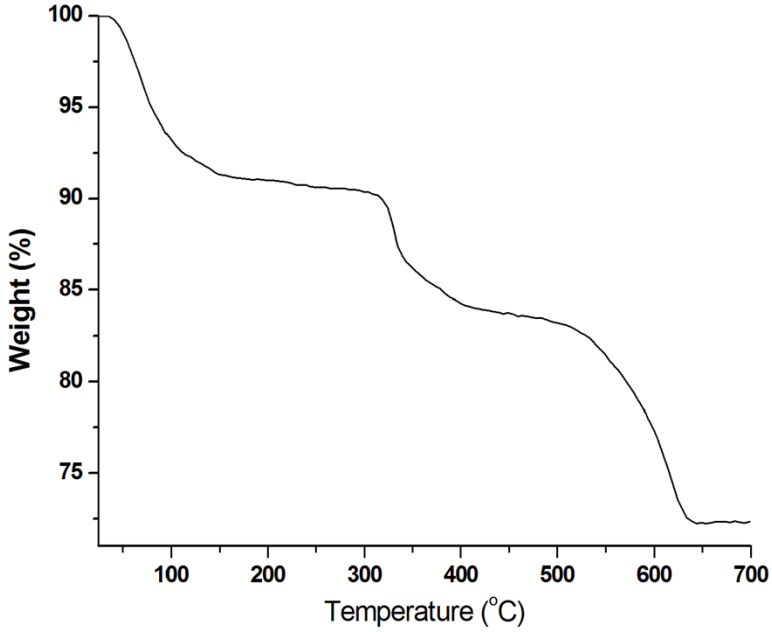

Figure S2. TG curve of compound **1**.

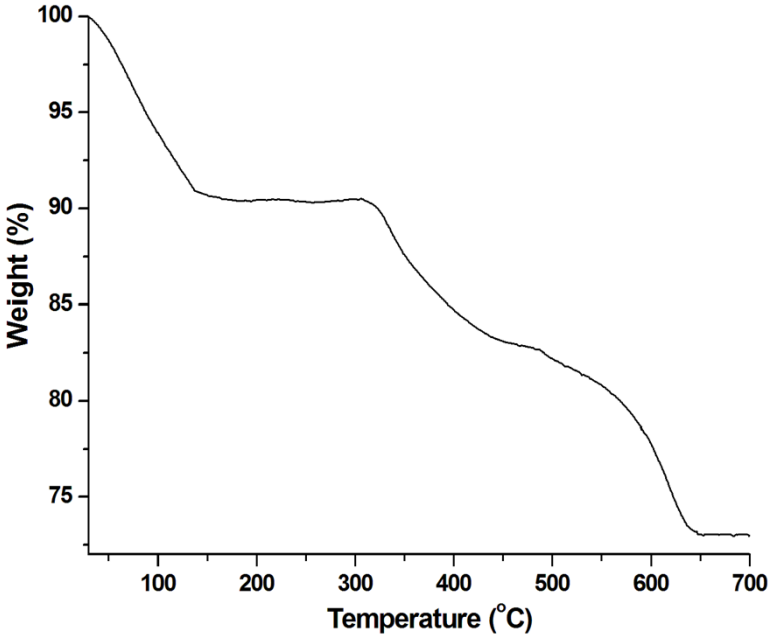

Figure S3. TG curve of **E1**.

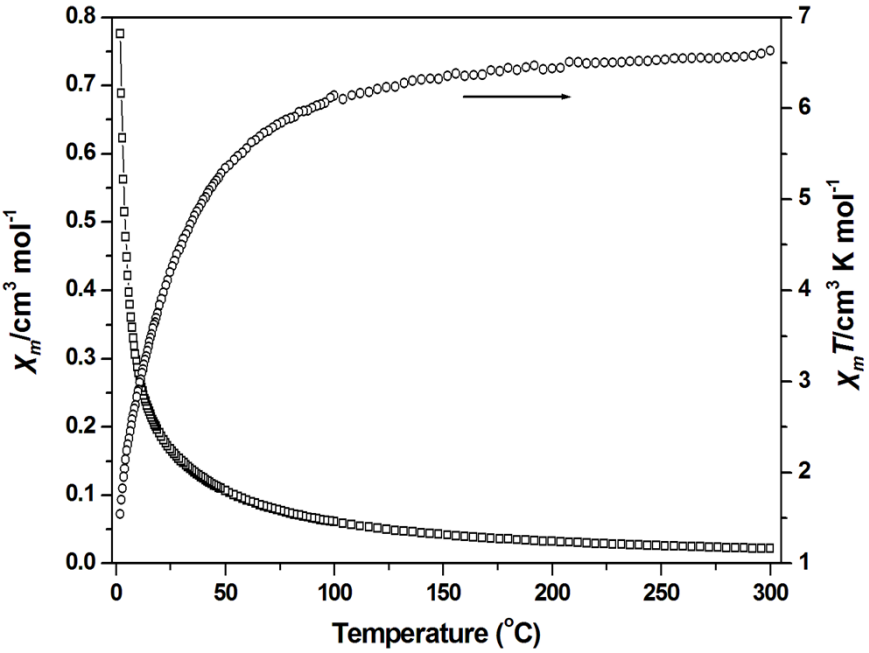

Figure S4. The temperature dependences of reciprocal magnetic susceptibility χ_M^{-1}(□) and the product $\chi_M T$ (o) for **1**.

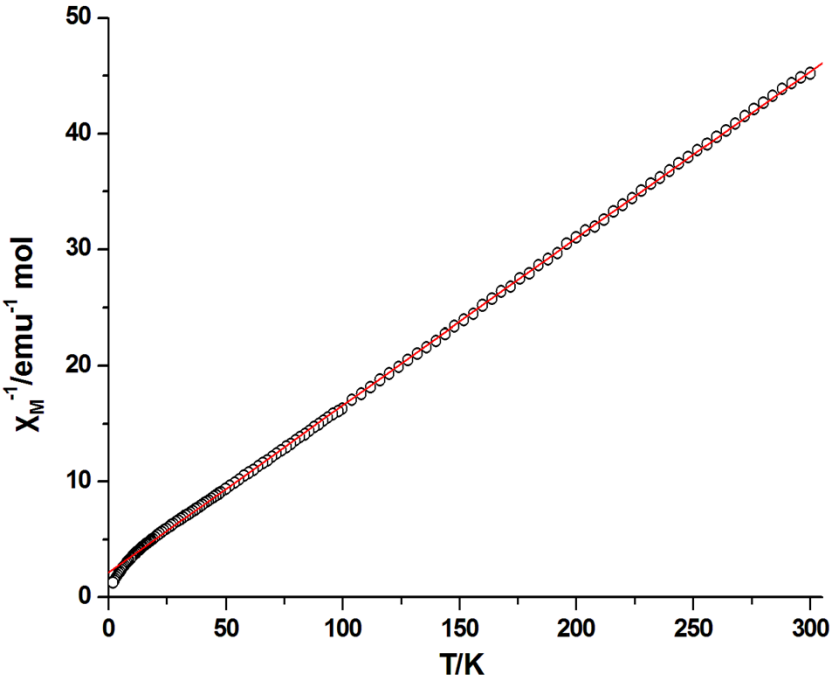

Figure S5. Temperature dependence of $\chi_m^{-1}$for **1**. The solid line is the best-fit according to the Curve-Weiss law.

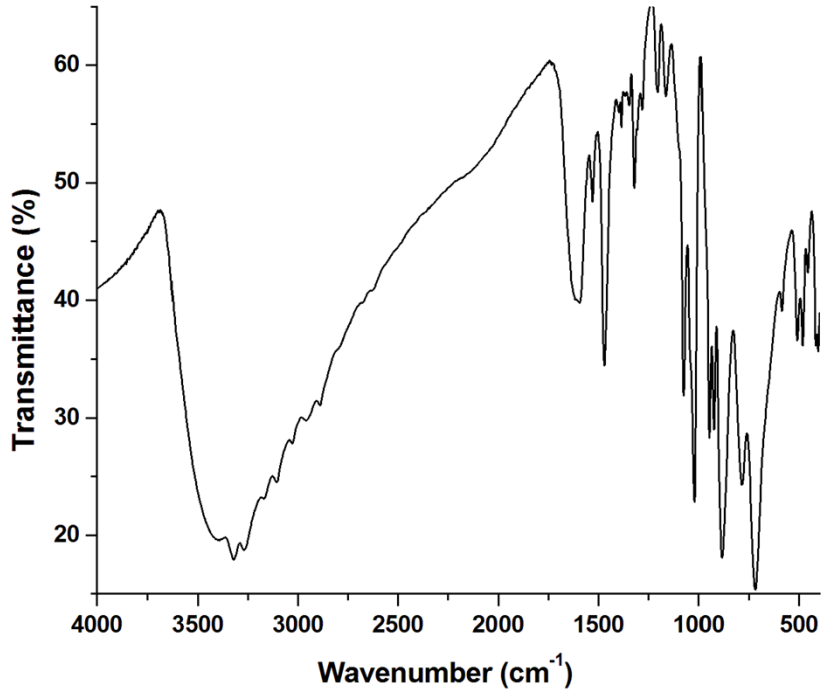

Figure S6. IR spectrum of **1**.

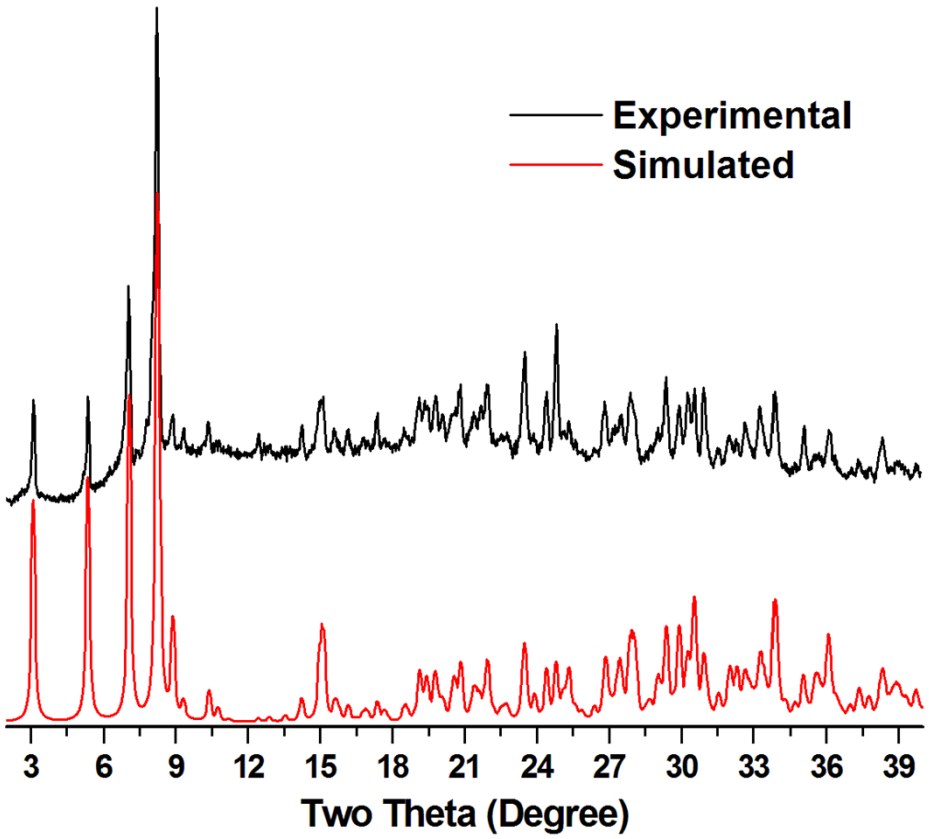

Figure S7. PXRD patterns of **1**, showing as-synthesized sample **1** is pure phase.

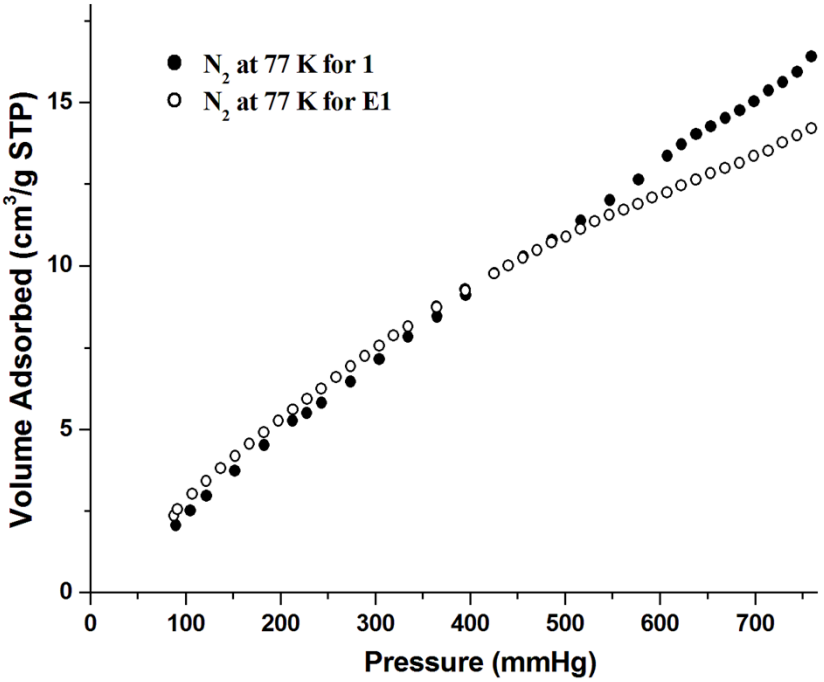

Figure S8. N_2 adsorption isotherms of **1** and **E1**.

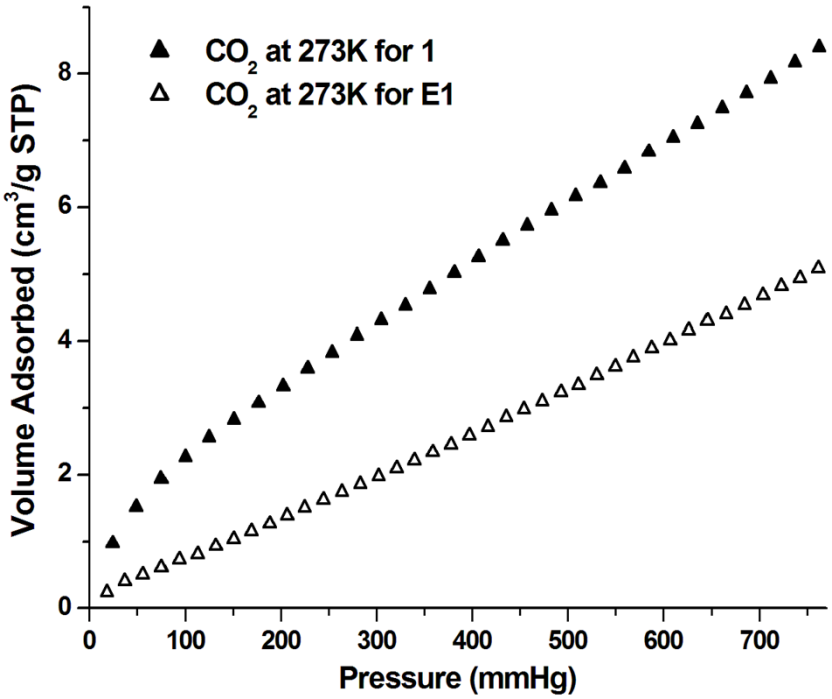

Figure S9. CO_2 adsorption isotherms of **1** and **E1**.

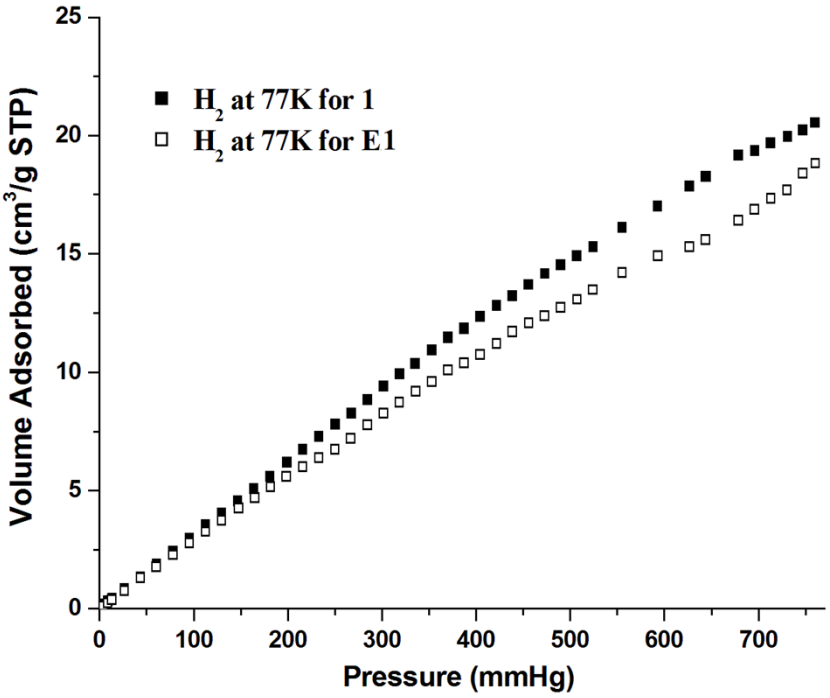

Figure S10. H_2 adsorption isotherms of **1** and **E1**.